CHIN. PHYS. LETT. Vol. 35, No. 2 (2018) 020701

Orbital Angular Momentum Generation Using Circular Ring Resonators in Radio Frequency *

Fu-Chun Mao(毛福春)[1], Ming Huang(黄铭)[1**], Cheng-Fu Yang(杨成福)[1],
Ting-Hua Li(李廷华)[2], Jia-Lin Zhang(张加林)[3], Si-Yu Chen(陈思宇)[1]

[1]*School of Information Science and Engineering, Yunnan University, Kunming 650091*
[2]*Center of China Tobacco Yunnan Industrial Co. Ltd. Kunming 65023*
[3]*Radio Monitoring Center of Yunnan Province, Kunming 650228*

(Received 31 October 2017)

Electromagnetic field generators based on circular ring resonators, whose perimeters are integer times of equivalent wavelength, are well known to have attractive potential for producing radio vortexes carrying orbital angular momentum (OAM). We study the radiation characteristics of the generators based on radiation vector and antenna array theory. The behaviors of radiation patterns, field intensity and phase distribution are investigated in detail, and show classical features of OAM beams. The evolution of the generators performance versus the OAM state is also analyzed. The proposed generators can be realized by all kinds of microwave transmission lines, verified by two different prototypes. The discussions and conclusions drawn in this study are useful and meaningful for the radio OAM generator design.

PACS: 07.57.Hm, 41.20.−q, 42.50.Tx DOI: 10.1088/0256-307X/35/2/020701

Researchers have great expectations for orbital angular momentum (OAM) to enhance the performances of future communication systems. One primary reason is that different OAM modes are mutually orthogonal, which makes it possible for OAM carriers to be multiplexed and demultiplexed. Thus the spectral efficiency and system capacity can be enormously increased.[1,2] For instance, in Ref. [3] a spectral efficiency of 435 bit×s^{-1}×Hz^{-1} was obtained, which is much higher than that of the typical LTE systems (16 bit×s^{-1}×Hz^{-1}).[4] However, there are also naysayers who argue that OAM is just a subset of multiple-input and multiple-output (MIMO) and therefore does not provide any additional capacity gain.[5,6] They employed the traditional methodology of MIMO systems to analyze the new OAM based systems, which eventually led to their conservative conclusions. Disputes between these two sides reveal that the prospect of OAM-based communication systems is far from settled yet.

Effective efforts towards the generation, manipulation, transmission and detection of OAM are urgently required to explore the OAM-based communication systems. Here we mainly focus on the techniques of OAM generation in radio frequency. To the best of our knowledge, there are about five schemes of OAM generators in radio band to date. The first is the circular phased antenna array,[7] which performs well in the mode reconfiguration. However, the geometrical complexity of such a generator is very high since a complex feed-network is necessary in this scheme. The second is the helical parabolic antenna,[8] which introduces a radial cut and a helix with surface pitch $h = l\lambda/2$ in standard parabolic reflector, where l and λ are the mode number and the wavelength, respectively. The helical parabolic antenna is simple in geometry, but incapable of reconfiguring the OAM mode due to its strong geometrical dependence. The third is the circular polarized patch.[9,10] This type of generator can reconfigure two OAM modes with opposite sign, i.e., l and $-l$, but the multiplexer is not easy to design using this method. The fourth is the circular travelling-wave antenna, which is fascinating with its simple geometry, and mode reconfiguration, but the radiation efficiency is often low.[11,12] The fifth is the spiral antenna which shows its appeal with the reconfiguration opportunities and broadband capacity.[13]

In this work, we investigate the circular ring resonators (CRR)-based OAM generator whose perimeter is integer times of the equivalent wavelength. Such a geometry is capable of reconfiguring the OAM modes with opposite sign. Analytic formulas of the generator will be derived using the theory of radiation vector and antenna array, and validated by two different prototypes.

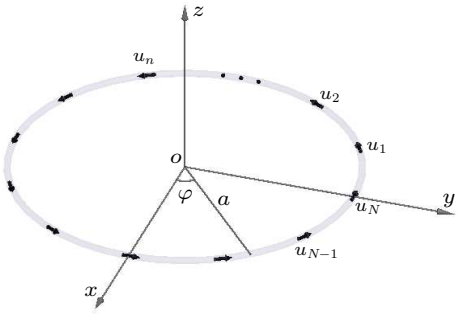


Fig. 1. Schematic representation of a CRR-based OAM generator.

The CRR loading a current $I_0 = 1/N$ can be regarded as a quasi-antenna array constituted by a series of tangential placed micro currents as shown in

*Supported by the National Natural Science Foundation of China under Grant No 61461052, the Specialized Research Fund for the Doctoral Program of Higher Education under Grant No 20135301110003, the Seventh of Yunnan University Graduate Student Scientific Research Project under Grant No ynuy201443, and the Doctoral Award for the Academic Newcomers (2014) of Yunnan Province under Grant No C6155501.

**Corresponding author. Email: huangming@ynu.edu.cn

© 2018 Chinese Physical Society and IOP Publishing Ltd

Fig. 1, where a, u_n and N are the generator radius, the azimuth of nth element and the elements number, respectively. Since the perimeter of CRR is l times of the waveguide wavelength, the micro current located at the nth node equals to $I_n = I_0 \exp(jlu_n)$. The generated field at $P(r,\theta,\phi)$ develops from the superposition and interference among the radiation of all micro currents, where $P(r,\theta,\phi)$ is an observation point in the far-field region. The array factor can be expressed as[14]

$$\begin{aligned} S(\theta,\phi) &= \sum_{n=1}^{N} I_n \exp[jka\sin\theta\cos(\phi-u_n)+jlu_n] \\ &= \frac{1}{N}\sum_{n=1}^{N} \exp[jka\sin\theta\cos(\phi-u_n)+jlu_n]. \quad (1) \end{aligned}$$

The limitations $N\to\infty$, $\Delta u_n = u_n - u_{n-1} = 2\pi/N \to du$ and $u_n \to u$ are used in the follow-up deduction. The radiated field is determined by the normalized radiation vector $\boldsymbol{F}(\theta,\phi)$, whose x, y, and z components are given as

$$\begin{aligned} F_x &= -S(\theta,\phi)\sin u_n \\ &= \frac{-1}{2\pi}\int_0^{2\pi} e^{j[l\phi+z\cos(\phi-u)]}\sin u du, \quad (2a) \\ F_y &= S(\theta,\phi)\cos u_n \\ &= \frac{1}{2\pi}\int_0^{2\pi} e^{j[l\phi+z\cos(\phi-u)]}\cos u du, \quad (2b) \\ F_z &= 0. \quad (2c) \end{aligned}$$

We first consider $F_x(\theta,\phi)$, which can be deduced by applying the integral formula of the Bessel function. The variable substitutions $q = ka\sin\theta$ and $v = u-\phi$ are employed. Then, we obtain

$$\begin{aligned} F_x(\theta,\phi) &= -\frac{e^{jl\phi}}{2\pi}\int_{-\phi}^{2\pi-\phi} e^{j(lv+z\cos v)}\sin(v+\phi)dv \\ &= -\frac{e^{jl\phi}}{2\pi}\int_{-\phi}^{2\pi-\phi}\{e^{j(lv+z\cos v)} \\ &\quad\cdot\frac{1}{2j}[e^{jv}-e^{-jv}]\cos\phi + e^{j(lv+z\cos v)} \\ &\quad\cdot\frac{1}{2}[e^{jv}+e^{-jv}]\sin\phi\}dv \\ &= e^{jl\phi}e^{j\pi l/2}\Big\{\frac{1}{2j}[J_{l+1}(q)e^{j\pi/2} \\ &\quad - J_{l-1}(q)e^{-j\pi/2}] + \frac{1}{2}[J_{l+1}(q)e^{j\pi/2} \\ &\quad + J_{l-1}(q)e^{-j\pi/2}]\Big\} \\ &= e^{jl(\phi+\pi/2)}\Big\{\frac{1}{2j}\cdot j[J_{l+1}(q)+J_{l-1}(q)] \\ &\quad + \frac{1}{2}\cdot j[J_{l+1}(q)-J_{l-1}(q)]\Big\} \\ &= e^{jl(\phi+\pi/2)}\Big[\frac{l}{q}J_l(q)\cos\phi - jJ_l'(q)\sin\phi\Big]. \end{aligned}$$

By following the same procedure, we obtain $F_y(\theta,\phi)$ as

$$F_y(\theta,\phi) = e^{jl(\phi+\pi/2)}\Big[jJ_l'(q)\cos\phi + \frac{l}{z}J_l(q)\sin\phi\Big]. \quad (3)$$

The θ and ϕ components of $\boldsymbol{F}$ can be expressed as $F_\theta = F_x\cos\theta\cos\phi + F_y\cos\theta\sin\phi - F_z\sin\theta$ and $F_\phi = -F_x\cdot\sin\phi + F_y\cdot\cos\phi$. Thus the expressions for F_θ and F_ϕ are obtained as

$$\begin{aligned} F_\theta(\theta,\phi) &= e^{jl(\phi+\pi/2)}\frac{l}{q}\cos\theta J_l(q), \quad (4a) \\ F_\phi(\theta,\phi) &= je^{jl(\phi+\pi/2)}J_l'(q). \quad (4b) \end{aligned}$$

Using the radiation vector, we can express the electric field as $\boldsymbol{E} = (jNkLI_0\eta/4\pi r)\cdot e^{-jkr}\cdot\boldsymbol{F}$ and the magnetic field as $\boldsymbol{H} = \eta^{-1}r^{-1}\vec{r}\times\boldsymbol{E}$, where η, L, and $\boldsymbol{r}$ denote the wave impedance of air, the length of single micro current and the position vector, respectively. Accordingly, the electric field in the form of spherical coordinate is obtained as

$$\begin{aligned} E_\theta &= e^{jl(\phi+\pi/2)}\frac{l}{q}\cos\theta J_l(q)\frac{jk60\pi a}{r}e^{-jkr}, \quad (5a) \\ E_\phi &= je^{jl(\phi+\pi/2)}J_l'(q)\frac{jk60\pi a}{r}e^{-jkr}. \quad (5b) \end{aligned}$$

The electric field in the form of cartesian coordinate can be expressed as

$$\begin{aligned} E_x &= e^{jl(\phi+\pi/2)}\Big[\frac{l}{q}J_l(z)\cos\phi \\ &\quad - jJ_l'(q)\sin\phi\Big]\frac{jk60\pi a}{r}e^{-jkr}, \quad (6a) \\ E_y &= e^{jl(\phi+\pi/2)}\Big[jJ_l'(q)\cos\phi \\ &\quad + \frac{l}{q}J_l(q)\sin\phi\Big]\frac{jk60\pi a}{r}e^{-jkr}. \quad (6b) \end{aligned}$$

From the above formula deductions, we can see that the radiated fields are characterized by a phase factor of $e^{jl(\phi+\pi/2)}$ and the Bessel functions ($J_l(\cdot)$ and $J_l'(\cdot)$). The phase factor $e^{jl(\phi+\pi/2)}$ enables the generated beam to have a screwy wave front with l spiral trajectories, which is one of the most essential features of the OAM beams. The Bessel functions make the produced waves behave as hollow beams, which is another typical characteristic of OAM beams.

Radiation patterns of the generators operating at different OAM states are calculated, as shown in Fig. 2, where $f_\varphi = |F_\phi|$, $f_\theta = |F_\theta|$. The radiation patterns in the vertical plane $\phi = 45°$ are shown in Figs. 2(a)–2(d). It is obvious that for the states $|l| = 1$, the maximum of f_φ as well as that of f_θ occurs at the direction of z-axis ($\theta = 0°$), which is different from the Laguerre–Gaussian beams.[15] In fact, the OAM beams with $|l| = 1$ degenerate as circularly polarized field here. For the states $|l| > 1$, the maxima of f_φ and f_θ deviate from the z axis. Furthermore, such deviation grows its scale along with the increase of $|l|$. The radiation patterns in the horizontal plane $\theta = 90°$ are shown in Figs. 2(e)–2(h). All generators provide good homogenous radiation in the horizontal direction.

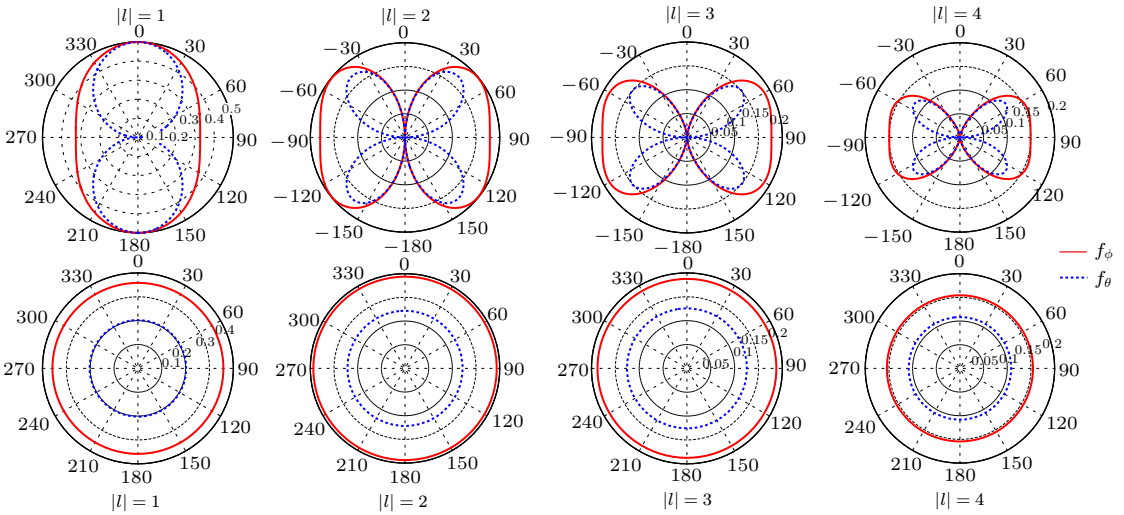


Fig. 2. Radiation patterns of the radiation vector.

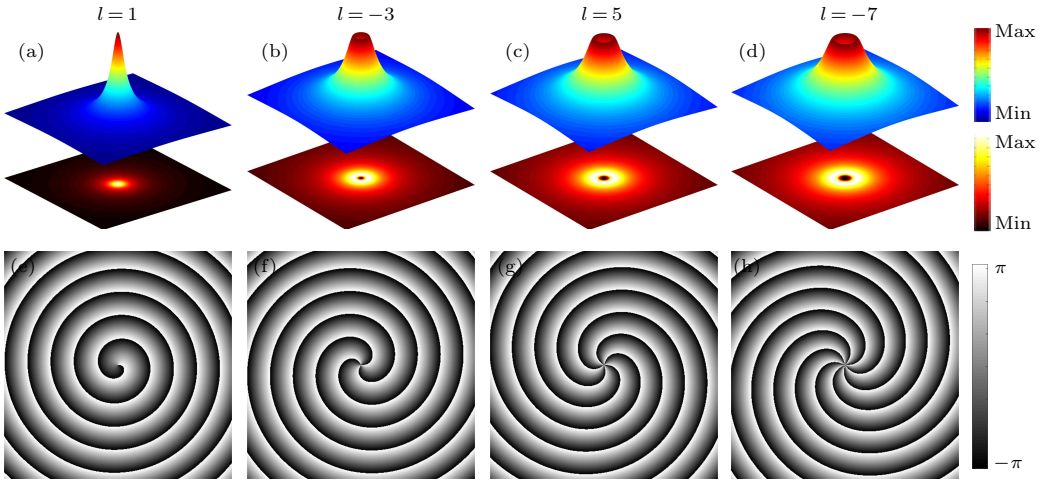


Fig. 3. The intensity and phase distribution of the electric field.

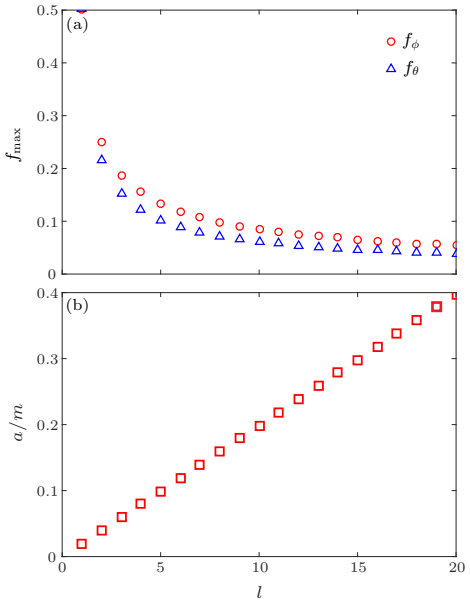


Fig. 4. Evolution of radiation vector and generator radius versus the mode number.

The intensity and phase distribution of electric field for the modes $l = 1, -3, 5, -7$ are depicted in Fig. 3. Theoretically, a can take any nonnegative value that would not lead to the failure of the aforementioned formulas. We consider the convenience of real fabrication and set $a = |l\lambda/2\pi|$. The different a makes it possible to nest multiple generators in the same plane to construct a simple multiplexer. It must be pointed out that the beam with $l = 0$ will not be produced via this setup as it calls for a zero-sized geometry. The intensity distribution of electric field is shown in Figs. 3(a)–3(d). It is obvious that the maximum radiation occurs exactly at the bore sight direction for the mode $l = 1$, while for the remaining modes the maximum radiation direction deviates from the bore sight direction and thus behaves like hollow beams. The equiphase patterns contain l Archimedean spirals as shown in Figs. 3(e)–3(h). Obviously, the number of spiral tracks in phase distributions is numerically equal to l, while the rotation direction of the spiral stands for the sign of OAM modes, i.e., the left-hand rotation for $+$, and the right-hand rotation for $-$.

Since the radius is controlled by $a = |l\lambda/2\pi|$, the increase of l will produce triple outcomes. The first

is the decrease of the radiation capacity (Fig. 4(a)). According to our calculations, when the generator works at modes $|l| = 1$, the maximum of f_φ, as well as f_θ, is 0.5. However, they will decrease to 0.054 and 0.037, respectively, when the generator works at modes $|l| = 20$. The second is the increase of the geometry dimension since a higher mode calls for a larger a (Fig. 4(b)). The variation of a is ruled by $a_l/a_{l-1} = l/(l-1)$. The third is the growth of intensity null spot in the boresight, which inevitably reduces the effective propagation distance of the OAM beams. Therefore, this kind of OAM generator is only advantageous to generate OAM beams with small-value l. In addition, the use of microwave transmission lines with small λ_e like microstrip, coplanar waveguide and slotline in the generator fabrication will be beneficial not only for the compactness and miniaturization, but also for the qualities of the radiated OAM beams.

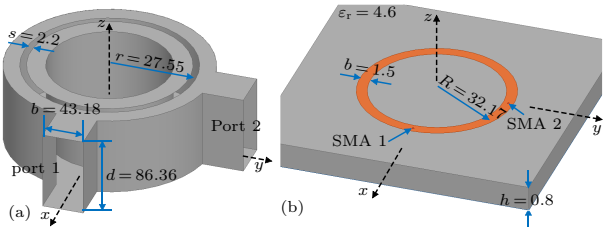


Fig. 5. Schematic diagrams of the two mentioned prototypes. (a) Generator works at modes based on rectangular waveguide; and (b) generator works on modes based on microstrip.

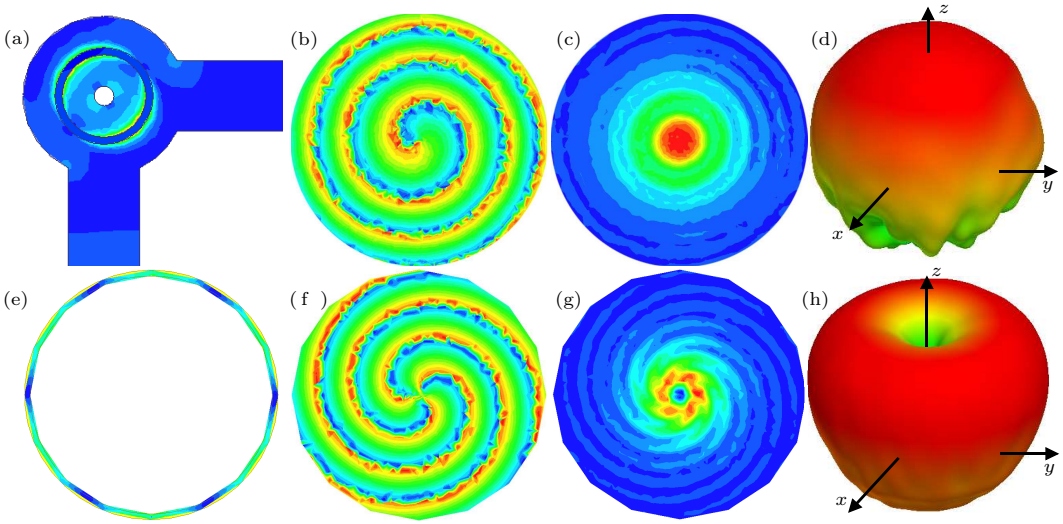


Fig. 6. Simulation results of the mentioned generators, where (a)–(d) are, respectively, the intensity of surface current, phase and intensity distribution of electric field, and 3D polar plot of gain for the generator depicted in Fig. 5(a). (e)–(f) The corresponding results for the generator shown in Fig. 5(b).

To verify the feasibility and flexibility of this type of OAM generator, we further designed and simulated two different prototypes. One of them is constructed by rectangular waveguide (Fig. 5(a)), while the other by microstrip (Fig. 5(b)). In Fig. 5, d and b ($d > b$) represent the dimensions of the rectangular waveguide, s denotes the width of slot, r is the radius of CRR, h and ε_r are the thickness and relative permittivity of dielectric substrate, w is the width of microstrip, and R is the radius of the microstrip CRR. The length unit is millimeters. Both generators work at $f = 2.452\,\text{GHz}$. The generators shown in Figs. 5(a) and 5(b) are designed to produce OAM beams with $|l| = 1$ and $|l| = 3$, respectively. Port 1 (or SMA 1) and port 2 (or SMA 2) are apart by $\pi/2$. Signals with equal magnitude are used to feed the generators through the ports (or SMAs). It should be pointed out that these generators generate OAM beams with left-hand spiral phase structure, i.e., $l = 1$ and $l = 3$, when the signal through port 2 (or SMA 2) lags the signal passing through port 1 (or SMA 1) by $\pi/2$, and vice versa.

The simulation results of surface current, phase and intensity of electric field, and three-dimensional polar plot of gain are shown in Fig. 6. Specifically, Figs. 6(a)–6(d) are for the generator portrayed in Fig. 5(a), while Figs. 6(e)–6(h) are for the generator depicted in Fig. 5(b). Clearly, both the generators have successfully achieved the intended function, i.e., the former and the latter radiate the OAM beam with $l = 1$ and $l = 3$, respectively. According to the calculations, the peak directivity and peak gain for both the generators are (6.2792, 2.5764) dB and (6.6164, 2.6733) dB, respectively. These results evidently reveal that the proposed CRR-based OAM generators can be implemented by varied microwave transmission lines.

In summary, the radiation properties of the CRR-based OAM generators have been analyzed based on the theory of antenna array and radiation vector. Theoretical equations of the radiation field are deduced. We find that the generated OAM beams belong to the Bessel beams with spiral wavefront. This type of OAM generator is suitable to generate OAM beams with small mode number and can be used to fabricate simple OAM multiplexer through nested arrangement. Since the CRR-based OAM generators can be manufactured flexibly by all kinds of microwave transmission lines, the deductions and discussions presented in this work are realistically helpful to research and appli-

cations of OAM-based technologies in various wireless systems.

References

[1] Willner A E, Huang H, Yan Y, Ren Y, Ahmed N, Xie G, Bao C, Li L, Cao Y, Zhao Z, Wang J, Lavery M P J, Tur M, Ramachandran S, Molisch A F, Ashrafi N and Ashrafi S 2015 *Adv. Opt. Photon.* **7** 66

[2] Bozinovic N, Yue Y, Ren Y, Tur M, Kristensen P, Huang H, Willner A E and Ramachandran S 2013 *Science* **340** 1545

[3] Wang J, Liu J, Lv X, Zhu L, Wang D, Li S, Wang A, Zhao Y, Long Y, Du J, Hu X, Zhou N, Chen S, Fang L and Zhang F 2015 *European Conference on Optical Communication* (Valencia Spain September 27–October 1 2015) p 1

[4] Parkvall S, Furuskär A and Dahlman E 2011 *IEEE Commun. Mag.* **49** 84

[5] Edfors O and Johansson A J 2012 *IEEE Trans. Antennas Propag.* **60** 1126

[6] Zhao N, Li X, Li G and Kahn J M 2015 *Nat. Photon.* **9** 822

[7] Thidé B, Then H, Sjöholm J and Palmer K 2007 *Phys. Rev. Lett.* **99** 087701

[8] Tamburini F, Mari E, Sponselli A and Thidé B 2012 *New J. Phys.* **14** 033001

[9] Chen J J, Lu Q N, Dong F F, Yang J J and Huang M 2016 *Opt. Express* **24** 11531

[10] Barbuto M, Trotta F, Bilotti F and Toscano A 2014 *Prog. Electromagn. Res.* **148** 23

[11] Zheng S L, Hui X N, Jin X F, Chi H and Zhang X M 2015 *IEEE Trans. Antennas Propag.* **63** 1530

[12] Hui X N, Zheng S L, Chen Y L, Hu Y P, Jin X F, Chi H and Zhang X M 2015 *Sci. Rep.* **5** 10148

[13] Mao F C, Huang M, Li T H, Zhang J L and Yang C F 2017 *Prog. Electromagn. Res.* **160** 19

[14] Knudsen H L 1953 *Proc. IRE* **41** 781

[15] Anguita J A, Herreros J and Djordjevic I B 2014 *IEEE Photon. J.* **6** 1